Proceedings of the ASME 2014 33rd International Conference on Ocean, Offshore and Arctic Engineering
OMAE2014
June 8-13, 2014, San Francisco, California, USA

OMAE2014-23981

A NUMERICAL STUDY ON STRATIFIED SHEAR LAYERS WITH RELEVANCE TO OIL-BOOM FAILURE

David Kristiansen

SINTEF Fisheries and Aquaculture AS
Trondheim, Norway
Email: david.kristiansen@sintef.no

Odd M. Faltinsen

Centre for Autonomous Marine Operations and Systems (AMOS),
Department of Marine Technology, NTNU
Trondheim, Norway
Email: odd.faltinsen@ntnu.no

ABSTRACT

Interface dynamics of two-phase flow, with relevance for leakage of oil retained by mechanical oil barriers, is studied by means of a 2D lattice-Boltzmann method combined with a phase-field model for interface capturing. A Multi-Relaxation-Time (MRT) model of the collision process is used to obtain a numerically stable model at high Reynolds-number flow. In the phase-field model, the interface is given a finite but small thickness where the fluid properties vary continuosly across a thin interface layer. Surface tension is modelled as a volume force in the transition layer. The numerical model is implemented for simulations with the graphic processing unit (GPU) of a desktop PC. Verification tests of the model are presented. The model is then applied to simulate gravity currents (GC) obtained from a lock-exchange configuration, using fluid parameters relevant for those of oil and water. Interface instability phenomena are observed, and obtained numerical results are in good agreement with theory. This work demonstrates that the numerical model presented can be used as a numerical tool for studies of stratified shear flows with relevance to oil-boom failure.

INTRODUCTION

The purpose of the present work is to develop a numerical tool that is adequate for modelling of two-fluid viscous flows in the context of oil containment failure of conventional oil booms. Mechanical oil barriers or oil ”booms” are still the most frequently used equipment for recovery of oil-spill floating on water [1]. Oil-booms can be placed at a site, e.g. around a ship wreck, or operated by one or more vessels. The efficiency of the boom as an oil recovery device is strongly dependent on the relative velocity between the oil-boom structure and the surrounding water. If the relative velocity between the contained oil and the water becomes too large, leakage of oil from the boom will occur. Such leakage can be caused by different physical effects, where also the physical properties of the oil play an important role. The chemical and physical character of oil in the sea will change with time due to weathering and emulsification processes [1]. A typical scenario is that both the viscosity and the density of the oil increase with time. Further, oil-water emulsions often show non-Newtonian behaviour, meaning that the viscosity depends on the applied shear rate. The most important failure-modes for oil booms, besides effects of wind and waves, are in the litterature defined as drainage, droplet entrainment and critical accumulation [2]. Drainage is a failure mode where low hydrodynamic pressure beneath the oil-boom creates a suction force on the oil close by the boom. Leakage occurs when this hydrodynamic suction force exceeds the buoyancy force on the oil, such that the local thickness of the oil-slick exceeds the barrier draft. A different failure mode that may occur for highly viscous oils is called critical accumulation, which is characterized by strong deformations of the oil-water interface followed by a massive loss of the contained oil [2]. Entrainment failure is a typical failure mode for light oils with low to moderate viscosity [3], where instabil-

Copyright © 2014 by ASME

Downloaded From: http://proceedings.asmedigitalcollection.asme.org/ on 12/08/2017 Terms of Use: http://www.asme.org/about-asme/terms-of-use

ities in the shear layer between the contained oil and the water, e.g. during towing of the boom, cause formation of oil droplets that are entrained from the oil-water interface. These oil droplets will in turn be advected by the surrounding water and escape under the boom. The density and viscosity of the oil, as well as the oil-water interfacial tension, are important parameters.

Instabilities of an interface separating two fluids, as those leading to entrainment failure, has been studied by many. The stability of stratified shear layers was investigated by Thorpe by means of theoretical work and physical experiments [4]. Kelvin-Helmholtz (KH) instabilities with the theoretical most unstable wavelength were observed when the relative velocity between the two fluids of the stratified shear layer exceeded a critical value. A different type of instability that was first described theoretically by Holmboe [5], is characterized by separation of free vortices from the interface shear layer into the bulk phases and formation of stationary or propagating wave disturbances at the interface. Such waves were later observed in physical experiments by Browand and Winant [6], who proposed the name Holmboe waves. A linear stability theory for stratified shear layers with a diffuse density interface was presented by Lawrence et al. [7], which could predict the different modes of the Holmboe instability. Investigations of Holmboe waves for immiscible fluids, both theoretical and experimental, were presented by Pouliquen et al. [8]. Turbulent mixing in stratified shear layers resulting from collapse of KH instabilities was studied numerically by Smyth and Moum [9]. Dynamics of oil-water interfaces in the context of oil-boom failure was investigated by Grilli et al. [10], where vortex-sheet models were developed to simulate an oil-slick contained by a boom. Their method proved to be able to model the oil-slick shape, including formation of KH-instabilities at the oil-water interface. Unfortunately, vortex-sheet models are not well suited for the study of entrainment failure as numerical breakdown is a typical consequence when massive changes of interface topology occur, as when the interface roll-up of the KH-instability collapses.

This paper is organized as follows. After the introduction, a newly developed numerical tool for simulation of two-phase incompressible viscous flows is described. Secondly, selected verifiation tests of the numerical model are presented. At the end, the numerical model is applied to stratified shear layers, and that produced by gravity currents obtained from a lock-exchange configuration are studied.

NUMERICAL MODEL

A numerical model for simulation of two-fluid incompressible viscous flow with relevance to oil-boom failure, is developed. Although oil-water emulsions of real oil slicks may show non-Newtonian behaviour, the present model is with Newtonian fluids. The model is based on the lattice-Boltzmann method (LBM), which has its theoretical basis from statistical mechanics and kinetic theory. In kinetic theory, the motion of a viscous fluid is described as a process of streaming and collisions of fictitous particles by means of particle probability density functions (PDF's) $h(\mathbf{x},\mathbf{c},t)$, which express the probability of finding a particle with a given velocity $\mathbf{c}$ at a given point in space $\mathbf{x}$ at time t. When h is known, macroscopic flow variables like velocity and density can be found as statistical moments of the PDF. In LBM, both the spatial dimensions and the space of particle velocities are discretized. A Cartesian grid is used for the spatial discretization, where the grid increment Δx is constant and equal for both directions. The velocity space is discretized with the D2Q9 stencil, where the nine discrete particle velocities are defined as

$$\mathbf{c}_i = \begin{cases} [0,0] & i=0 \\ [\cos((i-1)\pi/2), \sin((i-1)\pi/2)]c & i=1,2,3,4 \\ [\cos((2i-9)\pi/4), \sin((2i-9)\pi/4)]c\sqrt{2} & i=5,6,7,8 \end{cases} \tag{1}$$

where $c = \Delta x/\Delta t$ is the lattice speed and Δt is the time increment. This means that a particle will, if not being at rest, stream exactly to the nearest- or next-nearest (diagonal) grid points during one time step. Corresponding to each of the nine discrete particle velocities $\mathbf{c}_i$, with $i = 0,1,2,..,8$ is an unknown probability density function $h_i(\mathbf{x},t)$. Under given conditions of low Mach-number flow, LBM has shown to be consistent with the incompressible Navier-Stokes equations [11]. In the traditional LBM numerical scheme, the collision process is modelled as a time-relaxation of the density PDF towards a given equilibrium distribution function. This single-relaxation-time (SRT) model, also known as the BGK-model after the inventors Bhatnagar, Gross and Krook [12], yields an explicit numerical scheme for the unknown PDF's. Unfortunately, the SRT model is known to have issues with stability when applied to high Reynolds number flows. To improve numerical stability for high Reynolds numbes flows, a Multi-Relaxation-Time (MRT) collision model was developed by Lallemand and Luo [13]. The MRT collision model is used in the present scheme. No model is applied for eventual unresolved scales of turbulence.

Methods for simulation of multiphase flows can generally be divided into interface tracking methods where an evolution equation of the interface is solved, and interface capturing methods where the interface is reconstructed from some phase function. A phase-field model, which belongs to the latter group, is used in the present numerical model.

Phase-field model for two-phase flow

In phase-field models, the infinitely thin bounday of separation between two immiscible fluids is replaced by a transition region of finite thickness, where the phase concentration varies smoothly. Fluid parameters are described by the phase concentration and hence also have a continuous variation across the

Copyright © 2014 by ASME

Downloaded From: http://proceedings.asmedigitalcollection.asme.org/ on 12/08/2017 Terms of Use: http://www.asme.org/about-asme/terms-of-use

transition region. Surface tension is incorporated as a volume force in the interface region [14]. Phase-field models have been used with the Navier-Stokes equations for multiphase flow simulations, for which a detailed review is given by Jacqmin [15]. Temporal evolution of the phase concentration ϕ is given by an advection-diffusion equation known as the advective Cahn-Hilliard equation, which is the original equation defined by Cahn and Hilliard [16] with an advection term for the phase concentration included, i.e.

$$\frac{\partial \phi}{\partial t} + \mathbf{u} \cdot \nabla \phi = \nabla \cdot \left(M \nabla \mu_\phi \right). \tag{2}$$

The diffusion term is expressed as the gradient of the chemical potential μ_ϕ and the parameter M, which is the fluid mobility. Phase-field models are based on fluid free energy, which is a thermodynamic property of the fluid. A simple model of free energy density f is

$$f = \Psi(\phi) + \frac{1}{2}\kappa |\nabla \phi|^2, \tag{3}$$

where the first term on the right hand side is the bulk free energy, while the second term is the gradient energy or surface free energy. Further, κ is a measure of the surface free energy, which is related to surface tension. Two phases are possible if Ψ has two distinct minima. A chemical potential μ_ϕ is defined to be the variational derivative with respect to the phase concentration ϕ of the free energy functional $\mathscr{F}(\phi, \nabla\phi) = \int f \mathrm{d}V$, where the integration is over the whole volume occupied by the fluid [15]. This yields

$$\mu_\phi = \frac{\delta \mathscr{F}}{\delta \phi} = \Psi'(\phi) - \kappa \nabla^2 \phi. \tag{4}$$

The bulk free energy density is here given as a fourth order polynomial of the phase concentration as

$$\psi(\phi) = a\left(\phi^2 - \hat{\phi}^2\right)^2 \tag{5}$$

where $\hat{\phi} = (\rho_B - \rho_A)/2$ with ρ_A and ρ_B being the densities of the two fluids. Further, a is a constant related to surface tension and the interface thickness. Hence, the chemical potential is

$$\mu_\phi = 4a\phi\left(\phi^2 - \hat{\phi}^2\right) - \kappa \nabla^2 \phi \tag{6}$$

When the surface tension σ and interface width W are given, the parameters a and κ are found as

$$a = \frac{3\sigma}{4W\hat{\phi}^4}, \qquad \kappa = \frac{3\sigma W}{8\hat{\phi}^2} \tag{7}$$

The analytical solution of Eq. (2) for the phase concentration through the transition layer of a static flat interface is [15]

$$\phi(y) = \hat{\phi} \tanh\left(\frac{2(y-h)}{W}\right) \tag{8}$$

where y is a coordinate normal to an interface at $y = h$. The physical interface is taken as the zero-contour of the phase concentration ϕ.

The two-fluid LBM model

Coupled with the Navier-Stokes equations, phase-field methods have become increasingly popular for modelling complex interface flow phenomena [15]. Phase-field models have also been coupled with the lattice-Boltzmann method [17–19]. Here, we use the combined phase-field LBM model presented by Fakhari and Rahimian [18], where the governing hydrodynamic equation is based on the kinetic model for non-ideal fluids by He et al. [20] and where the transformation variable

$$f_i = c_s^2 h_i + w_i(p - \rho c_s^2) \tag{9}$$

is used to convert the particle density PDF h_i into a pressure PDF f_i. Here, p is the pressure and ρ is the density of the fluid, while w_i are weight coefficients to be defined later. This transformation was proposed by He et al. [21] in order to improve the numerical stability of their model when applied to multi-phase flow with large differences in mass density. The resulting lattice-Boltzmann equation, using Einstein notation, is

$$\begin{aligned} f_i(\mathbf{x}+\mathbf{c}_i\Delta t, t+\Delta t) - f_i(\mathbf{x}, t) = \\ -M_{ik}^{-1} S_{kj}\left(\left(\hat{f}_j(\mathbf{x},t) - \hat{f}_j^{eq}\right) + \frac{1}{2}\hat{F}_j^g\right) + F_i^g \end{aligned} \tag{10}$$

The first term on the right hand side models the particle collisions as a relaxation process of the distribution function $\hat{f}_j$ towards an equilibrium distribution function $\hat{f}_j^{eq}$ in moment space, according to the MRT-method [13], with S_{ij} being a diagonal matrix of relaxation-time coefficients. Here, we use $\mathbf{S} = \mathrm{diag}\{s_0, s_1, s_2, s_3, s_4, s_5, s_6, s_7, s_8\}$ with $s_0 = s_3 = s_5 = 1.0$, $s_1 = s_2 = s_4 = s_6 = 1.1$ and $s_7 = s_8 = 1/\tau$. The relaxation-time parameter s_7 determines the viscosity of the fluid, where the non-dimensional relaxation-time τ is related to the kinematic viscosity ν as $\tau = \nu/(c_s^2 \Delta t) + 1/2$. Here, $c_s = \Delta x/(\Delta t\sqrt{3})$ is a pseudo sound speed also called the *lattice sound speed*. The transformation from particle velocity space to moment space (indicated by a hat) is done with the transformation matrix $\mathbf{M}$ (see [13] for definition) as

$$\hat{f}_i = M_{ij} f_j, \qquad \hat{f}_i^{eq} = M_{ij} f_j^{eq}, \qquad \hat{F}_i^g = M_{ij} F_j^g \tag{11}$$

Copyright © 2014 by ASME

Downloaded From: http://proceedings.asmedigitalcollection.asme.org/ on 12/08/2017 Terms of Use: http://www.asme.org/about-asme/terms-of-use

The term F_g, which includes the effect of particle accelerations due to volume forces acting on the fluid particles, is

$$F_i^g = \frac{(\mathbf{c}_i - \mathbf{u})}{\rho} \cdot \left\{ (\mathbf{F}_s + \mathbf{F}_b) h_i^{eq} + \left(h_i^{eq} - w_i \rho \right) \nabla (\rho c_s^2) \right\} \Delta t. \quad (12)$$

These volume forces are, per unit volume, the gravitational force $\mathbf{F}_b = \rho \mathbf{g}$ and the surface tension force $\mathbf{F}_s = \mu_\phi \nabla \phi$ defined in terms of the free energy potential μ_ϕ and the phase concentration ϕ. Further, h_i^{eq} is the equilibrium distribution function corresponding to the discrete particle velocity $\mathbf{c}_i$ which reads

$$h_i^{eq} = w_i \rho \left(1 + \frac{\mathbf{c}_i \cdot \mathbf{u}}{c_s^2} + \frac{(\mathbf{c}_i \cdot \mathbf{u})^2}{2c_s^4} - \frac{\mathbf{u} \cdot \mathbf{u}}{2c_s^2} \right). \quad (13)$$

Here, w_i are weight coefficients where $w_0 = 4/9$, $w_{1,2,3,4} = 1/9$ and $w_{5,6,7,8} = 1/36$. These weight coefficients can be related to a Gauss-Hermite quadrature for evaluation of statistical moments of the Maxwell-Boltzmann distribution [22]. The Mach-number is defined in terms of the pseudo sound speed as $\mathrm{Ma} = u/c_s$ with u being the macroscopic fluid velocity. Similarly as the transformation of the traditional density distrubution function h_i to the pressure distribution function f_i defined in Eq. 9, a modified equilibrium distribution function is obtained by the transformation $f_i^{eq} = c_s^2 h_i^{eq} + w_i(p - \rho c_s^2)$. When the distribution functions f_i for a new time step are found, the macroscopic fluid conditions (pressure p and velocity $\mathbf{u}$) are calculated as statistical moments of the distribution function as

$$p = \sum_{i=0}^{8} f_i + \frac{\Delta t}{2} \mathbf{u} \cdot \nabla \left(\rho c_s^2 \right) \quad (14)$$

$$\mathbf{u} = \frac{1}{\rho c_s^2} \sum_{i=0}^{8} \mathbf{c}_i f_i + \frac{\Delta t}{2\rho} \left(\mathbf{F}_s + \mathbf{F}_b \right) \quad (15)$$

The local mass density and kinematic coefficient is found from the phase concentration parameter as

$$\rho = \rho_1 + \frac{\phi + \hat{\phi}}{2\hat{\phi}} (\rho_2 - \rho_1), \qquad \nu = \nu_1 + \frac{\phi + \hat{\phi}}{2\hat{\phi}} (\nu_2 - \nu_1) \quad (16)$$

The generalized LBE for the phase evolution is

$$g_i(\mathbf{x} + \mathbf{c}_i \Delta t, t + \Delta t) = g_i(\mathbf{x}, t) - \frac{(g_i - g_i^{eq})}{\tau_g} \quad (17)$$

where τ_g is the relaxation time coefficient. The equilibrium distribution function proposed by Huang et al. [17] is

$$g_i^{eq} = \begin{cases} \phi - \tilde{M} \mu_\phi (1 - w_0)/c_s^2, & (i = 0) \\ w_i [\tilde{M} \mu_\phi + \phi (\mathbf{c}_i \cdot \mathbf{u})]/c_s^2, & (i > 0) \end{cases} \quad (18)$$

where the parameter $\tilde{M}$ is used to control the mobility through the relation $M = (\tau_g - 1/2)\tilde{M}\Delta t$. When the new values of the phase distribution function is found, the phase concentration is obtained as

$$\phi = \sum_{i=0}^{8} g_i \quad (19)$$

The phase concentration ϕ in the transition layer is initialized according to Eq. (8). Spatial oscillations of the phase concentration may occur near the interface due to steep gradients. Hence, bounds on ϕ are used when evaluating the fluid density and viscosity to avoid unphysical values with subsequent numerical instabilities. Another numerical phenomenon is spurious velocities, which are unphysical currents that can occur at the interface between the two phases in a simulation. Such spurious velocities are nearly eliminated by modified stencils for evaluating numerical derivatives [23] of the phase concentration ϕ.

$$\nabla \phi|_{(\mathbf{x})} = \frac{3}{\Delta x} \sum_i w_i \mathbf{c}_i \phi (\mathbf{x} + \mathbf{c}_i \Delta t) \quad (20)$$

$$\nabla^2 \phi|_{(\mathbf{x})} = \frac{6}{\Delta x^2} \sum_i w_i \left[\phi (\mathbf{x} + \mathbf{c}_i \Delta t) - \phi (\mathbf{x}) \right] \quad (21)$$

This is used for evaluation of $\nabla^2 \phi$ in Eq. (6) and for evaluation of $\nabla \rho$ in Eqs. (12) and (14). Note that by definition, $\nabla \rho = \nabla \phi$.

GPU implementation

The fact that the governing equation of LBM is explicit makes the numerical scheme highly suitable for parallel computations. To utilize this, the present model is implemented for parallel execution on graphic processing units (GPU's) using CUDA. To achieve good performance of the present GPU-code, the number of global memory access on the GPU and copy of memory from GPU-RAM to CPU-RAM is kept as low as possible. The parallel executions are distributed over a grid of process threads, where one process thread is assigned to each point on the computational grid. The array of simulation variables, which are the probaility density functions (PDF's), is organized in a row-major order as follows

```
PDF[irow*NumCols + icol + alpha*NumRows*NumCols]
```

where *irow* and *icol* refer to the spatial row index and column index, respectively. This ensures that the PDF for a given lattice link *alpha* for neighbour grid-points also are close in memory.

Copyright © 2014 by ASME

Downloaded From: http://proceedings.asmedigitalcollection.asme.org/ on 12/08/2017 Terms of Use: http://www.asme.org/about-asme/terms-of-use

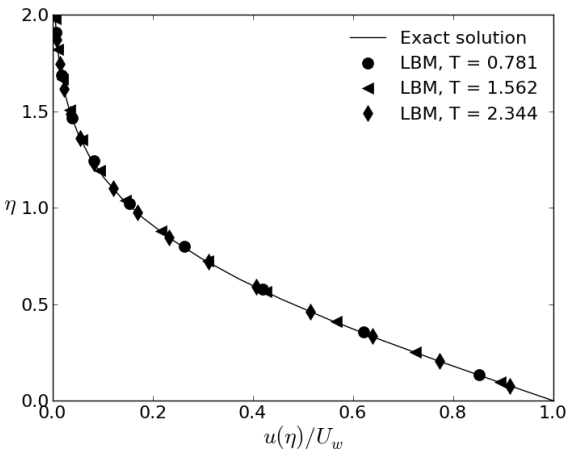

FIGURE 1: STOKES FIRST PROBLEM. COMPARISON OF VELOCITY PROFILE OBTAINED FROM PRESENT NUMERICAL SIMULATIONS WITH THEORETICAL PROFILE FOR NON-DIMENSIONAL TIMES $T = tU^2/\nu$.

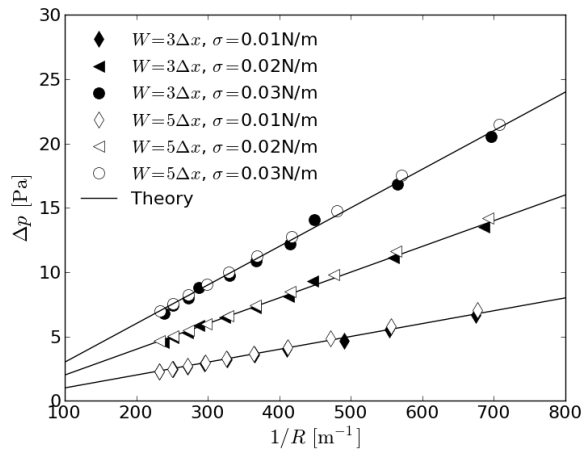

FIGURE 2: PRESSURE DIFFERENCE INSIDE AND OUTSIDE A STATIONARY BUBBLE. COMPARISON BETWEEN NUMERICAL SIMULATIONS AND THEORY.

VERIFICATION STUDIES

Stokes first problem

To verify that viscous effects are correctly modelled, the development of a laminar boundary layer above a no-slip wall suddenly set into tangential motion is considered. This is also known as the Stokes first problem (see e.g. Schlichting and Gersten [24]), for which an analytic solution to the linearized Navier-Stokes equations exists. The tangential velocity u relative to the wall velocity U_w is given as a function of the normal distance to the wall y, and time t as $u(y,t) = U_w \exp(-\eta(y,t))$, where $\eta = y/(2\sqrt{\nu t})$ is the similarity parameter. As usual, ν is the kinematic viscosity coefficient. Obtained numerical results for the velocity profile inside the laminar boundary layer are in good agreement with theory as shown in Fig.1, where the normalized error $\varepsilon = \exp(-\eta) - u/U_w$ is less than 1%.

Stationary bubble

A much used test for verification of surface tension models is the case of a stationary bubble. Due to surface tension, the pressure inside the bubble is larger than outside. The theoretical pressure difference across the interface is given by Laplace law as $p_{in} - p_{out} = \sigma/R$, where σ is the interfacial tension and R is the bubble radius. Numerical simulations were performed for various values of σ and R. Two different values of the interface thickness, $W = 3\Delta x$ and $W = 5\Delta x$ were also tested. The bubble was located in a square domain with side dimensions $L = H = 0.031$ m, that was discretized with 128 grid points in each direction. The density inside the bubble was $\rho_1 = 980\,\mathrm{kg/m^3}$, while the density of the surrounding fluid was $\rho_2 = 1000\,\mathrm{kg/m^3}$. The mobility parameter was set to $\tilde{M} = 200$ for all simulations. A uniform pressure distribution was used as initial condition. This resulted in a transient fluid motion due to the initial imbalance of forces from surface tension and the jump in pressure across the surface of the bubble. The length of each simulation was 200,000 timesteps with time increment $\Delta t = 1.0 \times 10^{-4}$ s, which was sufficient for all transients to die out. To evaluate the pressure difference across the bubble boundary, grid points along a straight line through the domain and through the center of the bubble was considered. The inside pressure was taken as the average pressure of the grid points on this line for which the phase concentration $\phi > 0.95\hat{\phi}$. Similarly was the outside pressure evaluated as the average pressure for the points on the line where $\phi < -0.95\hat{\phi}$. The corresponding bubble radius was found from the zero-contour of the phase concentration ϕ. Obtained results are summarized and compared with theory in Fig. 2.

Internal standing wave

Simulations with internal standing waves in a narrow channel was performed for verification of the numerical model. The upper and lower boundary of the channel was located at a distance $y = \pm h$ from the calm interface. The combined effect of gravity and surface tension on the wave frequency ω of a sinusoidal perturbation of the interface was investigated for various wavelengths λ. The theoretical dispersion relation for an internal gravity-capillary wave (see e.g. Lamb [25], p.459) are modified for the wall-boundaries at $y = \pm h$ to give

$$\omega^2 = \left(\frac{\rho_2 - \rho_1}{\rho_2 + \rho_1} gk + \frac{\sigma k^3}{\rho_2 + \rho_1}\right) \tanh(kh), \qquad (22)$$

Copyright © 2014 by ASME

Downloaded From: http://proceedings.asmedigitalcollection.asme.org/ on 12/08/2017 Terms of Use: http://www.asme.org/about-asme/terms-of-use

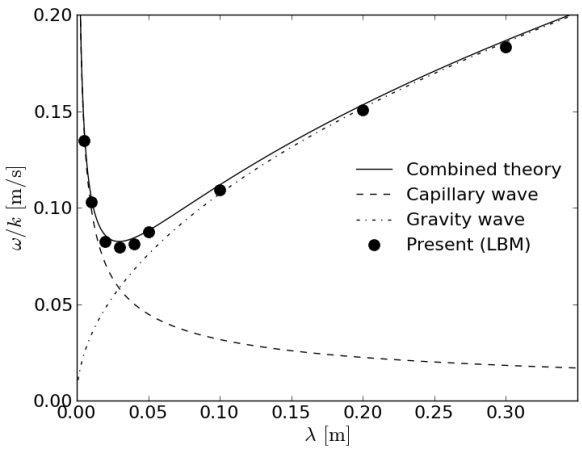

FIGURE 3: WAVE CELERITY FOR GRAVITY CAPILLARY WAVES. COMPARISON BETWEEN NUMERICAL SIMULATIONS AND THEORY.

where $k = 2\pi/\lambda$ is the wavenumber and g is the acceleration of gravity. The width and height of the computational domain were both one wavelength, which implies that $h = \lambda/2$. A sinusoidal wave perturbation of the interface with amplitude $\zeta_A = 0.025\lambda$ was used as initial condition. No-slip boundary conditions were imposed on the upper and lower boundaries, while periodic boundary conditions were used on the side boundaries. The domain was discretized with 256 grid points in each direction. Interface thickness of the phase-field model was set to $W = 3\Delta x$, while the mobility parameter was $\tilde{M} = 100$. Kinematic viscosity coefficient was $\nu = 10^{-6}\mathrm{m}^2/\mathrm{s}$ for both phases. The mass densities were $\rho_1 = 862.2\mathrm{kg/m}^3$ and $\rho_2 = 1000\mathrm{kg/m}^3$, i.e. representative for oil and fresh water. Wave frequencies obtained from the simulations divided by the corresponding wavenumber of the perturbation are compared with theory in Fig. 3. The present numerical results are in good agreement with the theoretical predictions with Eq. (22), although the obtained wave frequency from the simulations are slightly lower than the theoretical value. The largest deviation is obtained for the smallest wavelength, where the relative deviation of wave frequency is 6.6%. For the rest of the simulated cases, the relative deviation of the wave frequency is between 1% and 4%.

STUDIES OF STRATIFIED SHEAR LAYERS

The present numerical model is applied to study stratified shear layers, which has relevance to entrainment failure of oil booms. It is well known that perturbations of the interface of a stratified shear layer are unstable under certain conditions. In the presence of surface tension σ, stationary perturbations of a vortex sheet are found to be unstable if the relative velocity ΔU across the shear layer exceeds a critical value (see e.g. [4]), for which wave perturbations will grow into Kelvin-Helmholtz vortices. A different type of instability called Holmboe modes can occur if the velocity profile has a continuous variation across the interface with a finite thickness of the velocity gradient layer. Such stratified shear layers can develop due to viscous diffusion at the interface. An important parameter that characterizes the flow of stratified shear layers is the modified Richardson number

$$J = \frac{g_r l}{U^2} \tag{23}$$

where $g_r = g(\rho_2 - \rho_1)/\rho_2 = g(1-\gamma)$ is the reduced gravity, $l_c = \sqrt{\sigma/(g(\rho_2-\rho_1))}$ is the capillary length scale and $U = \Delta U/2$. The characteristic thicknesses d and δd of the diffusive layers on the two sides of the interface shear layer evolve as $d \sim \sqrt{\nu_1 t}$ and $\delta d \sim \sqrt{\nu_2 t}$, where ν_1 and ν_2 are the kinematic viscosities for the lighter fluid and the heavy fluid, respectively. Hence, an asymmetry of the velocity profile relative to the density interface develops if the kinematic viscosity of the two fluids are different. The asymmetry parameter is defined as [8]

$$\beta = \frac{1-\delta\rho_2/\rho_1}{1+\delta\rho_2/\rho_1} \tag{24}$$

where $\delta = \sqrt{\nu_2/\nu_1}$, such that the fluid velocity at the density interface is βU. A linear stability theory for stratified shear layers with immiscible fluids was presented by Pouliquen et al. [8], where the wave speed of a sinusoidal perturbation with wavelength λ is given by a fourth order characteristic equation with coefficients expressed in terms of J, β, $\hat{d} = d/l_c$, in addition to the non-dimensional perturbation wave number $\hat{k} = (2\pi/\lambda)l_c$. The complex roots of this characteristic equation is used to predict the different instability modes of the stratified shear layer.

Simulations of instability-modes

In order to investigate the instability modes of stratified shear layers, 2D numerical simulations of such flows in a narrow channel were performed. A rectangular domain of length $L = 0.12$ m and height $H = 0.03$ m was considered, where the upper and lower half of the domain was occupied by a lighter fluid with density $\rho_1 = 862.2\,\mathrm{kg/m}^3$ and a heavy fluid with density $\rho_2 = 1000\,\mathrm{kg/m}^3$, respectively. Both fluids had a kinematic viscosity coefficient of $\nu = 10^{-6}\,\mathrm{m}^2/\mathrm{s}$. A stratified shear layer was obtained by giving the upper and lower fluid a uniform but oppositely directed current velocity U, such that the relative velocity initially was $\Delta U = 2U$. Further, a sinusoidal wave perturbation was applied to the interface separating the two fluids, described by $\eta(x) = \eta_a \sin(kx)$ with η_a begin the initial amplitude

Copyright © 2014 by ASME

Downloaded From: http://proceedings.asmedigitalcollection.asme.org/ on 12/08/2017 Terms of Use: http://www.asme.org/about-asme/terms-of-use

and $k = 2\pi/\lambda$ the perturbation wave number. The wavelength of the perturbation was $\lambda_f = 0.03\,\mathrm{m}$. No-slip wall boundary condition was applied on the upper boundary and the lower boundary, while periodic boundary conditions were applied on the side boundaries. The domain was discretized by 1024 grid points in the horisontal direction and 256 grid points in the vertical direction, which is found to be sufficient to resolve the flow. Time-increment was set to $\Delta t = 5 \times 10^{-6}\,\mathrm{s}$. Two series where the velocity was varied from $U = 0.1\,\mathrm{m/s}$ to $U = 0.19\,\mathrm{m/s}$ were tested. One series was with surface tension $\sigma = 0.005\,\mathrm{N/m}$ and one was with $\sigma = 0.01\,\mathrm{N/m}$. Hence, the modified Richardson number was $0.07 < J < 0.26$ with $\sigma = 0.005\,\mathrm{N/m}$ and $0.10 < J < 0.37$ with $\sigma = 0.01\,\mathrm{N/m}$. For the case when $\sigma = 0.005\,\mathrm{N/m}$ and $U = 0.17\,\mathrm{m/s}$, we have $J = 0.09$, $\hat{k} = 0.4$, $\beta = 0$ and $\hat{d} = 0.09$, which yields pure imaginary roots of the characteristic equation where two of the resulting wave speeds have a positive imaginary part. This means stationary unstable KH-modes. KH-instability was also observed in numerical simulations with the given parameters as shown in Fig. 4a. When the velocity is reduced to $U = 0.1\,\mathrm{m/s}$, while keeping the other parameters constant, the Richardson number is increased to $J = 0.26$. The linear stability theory predicts two unstable waves propagating in opposite directions, i.e. symmetric Holmboe waves, when the non-dimensional thickness of the diffusive layer in each fluid is around $\hat{d} = 0.1$. This corresponds to a 10 % increase of the diffusive layer thickness d, which is easily obtained by viscous diffusion. Symmetric Holmboe waves are also observed in the numerical simulations (Fig. 4b). When the kinematic viscosity in the upper fluid is increased to $10^{-5}\,\mathrm{m^2/s}$, the asymmetry parameter is $\beta = -0.57$ and the asymmetric Holmboe instability mode is predicted with the stability theory, where the wave disturbances travel in the direction of the less viscous fluid. This is also in agreement with results from simulations (see Fig. 4c).

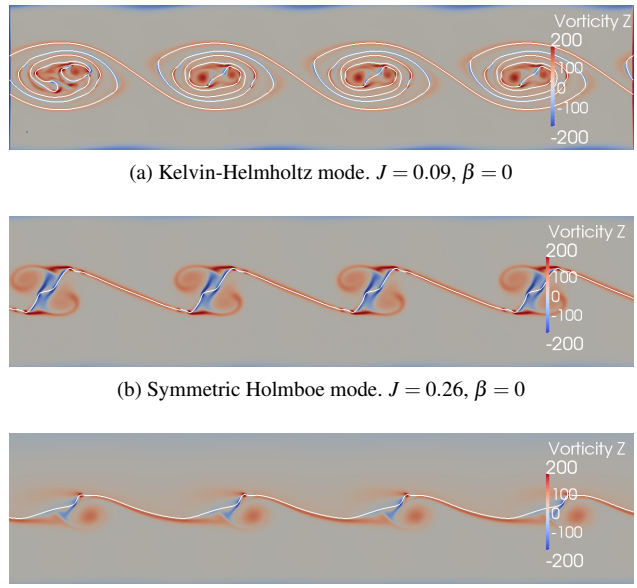

(a) Kelvin-Helmholtz mode. $J = 0.09$, $\beta = 0$

(b) Symmetric Holmboe mode. $J = 0.26$, $\beta = 0$

(c) Asymmetric Holmboe mode. $J = 0.26$, $\beta = -0.57$

FIGURE 4: VORTICITY FIELD IN UNITS OF s^{-1} FOR DIFFERENT INSTABILITY MODES OF STRATIFIED SHEAR LAYERS. THE INTERFACE IS SHOWN AS A SOLID LINE.

Simulations of gravity currents by lock-exchange

The contained oil of an oil-boom in operation has several similarities with a gravity current (GC), which can be described as a horizontal fluid flow resulting from gravity acting on two fluids with different density in a non-equilibrium configuration. The typical shape of a GC where a light fluid flows on top of a heavy fluid is characterized by an increased thickness of the front, referred to as the head of the GC. Lock-exchange is a configuration where a rectangular tank is divided into two chambers by a vertical barrier and where the density of the fluids contained in each of the two chambers are different. The experiment is started by removing the barrier.

Simulations of gravity-currents resulting from a lock-exchange configuration is performed for a series of density ratios $0.870 < \gamma < 0.993$, which are relevant density ratios for entrainment failure of oil-booms [2]. The actual densities of the two fluids and the dimensions of the domain were taken as those of the experiments by Lowe et al [26], where the length and height of the tank was $L = 1.8$ m and $H = 0.2$ m, respectively. The fictitious lock was placed at $x = 0$, i.e. half-way between the side boundaries at $x = \pm L/2$, and the domain was initialized with a heavy fluid for $x < 0$ and a lighter fluid at $x > 0$. The computational domain was discretized by 2304 and 256 grid points in the horizontal and vertical direction, respectively. Two series of simulations were run; one where the kinematic viscosities in the two fluids were equal to that of fresh water, i.e. $\nu_1 = \nu_2 = 10^{-6}\,\mathrm{m^2/s}$, and one where the kinematic viscosity of the light fluid was increased to $\nu_1 = 10^{-5}\,\mathrm{m^2/s}$. For all these tests, the surface tension was $\sigma = 0.03\,\mathrm{N/m}$. Further, the thickness of the density transition interface was set to $W = 3\Delta x$, while the mobility control parameter was $\tilde{M} = 200$. The velocity interface was initialized using the same variation and thickness as the density interface. Selected results are presented in Fig. 5 as snapshots of the vorticity-field.

Results and discussion

For the test with density ratio $\gamma = 0.993$ and $\nu_1 = \nu_2$ (Fig. 5a), the interface at the early stage of the simulation is characterized by the instable growth of two wave disturbances. These waves grow as the simulation proceeds, until they merge into a single wave profile. This wave profile is then dispersed into several wave disturbances. Plots of the vorticity field for the case of equal kinematic viscosities reveal that vorticity is shed from

Copyright © 2014 by ASME

Downloaded From: http://proceedings.asmedigitalcollection.asme.org/ on 12/08/2017 Terms of Use: http://www.asme.org/about-asme/terms-of-use

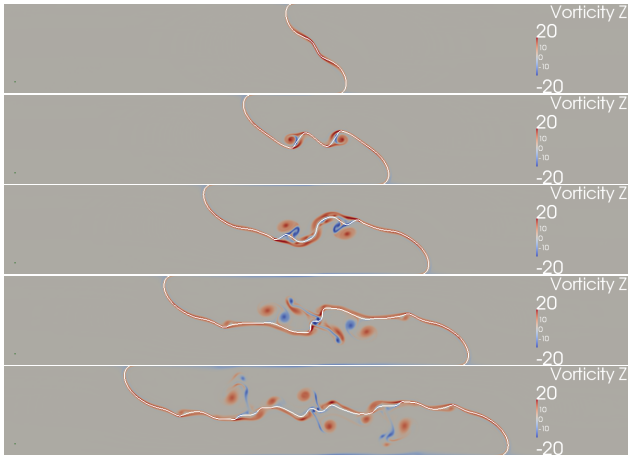

(a) $\gamma = 0.993$, $\beta = 0$

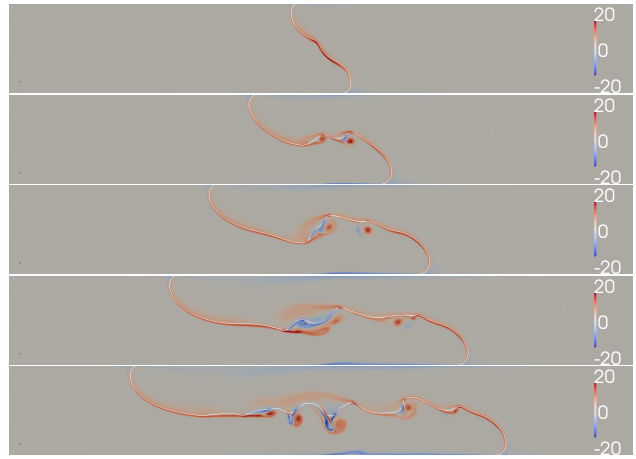

(b) $\gamma = 0.993$, $\beta = -0.57$

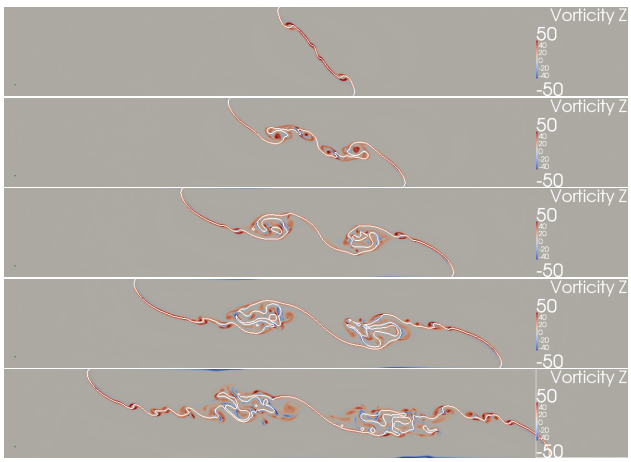

(c) $\gamma = 0.950$, $\beta = 0$

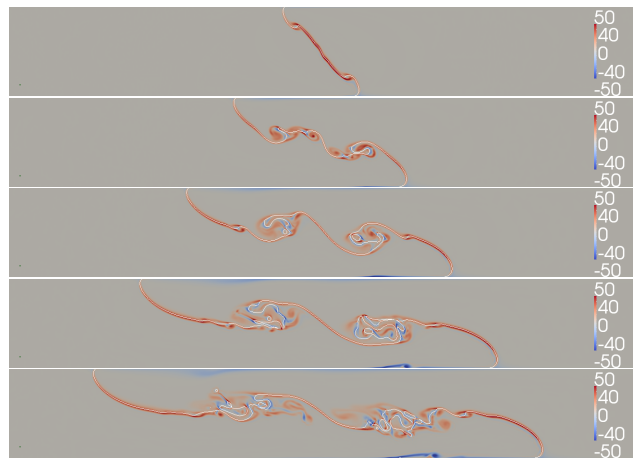

(d) $\gamma = 0.950$, $\beta = -0.57$

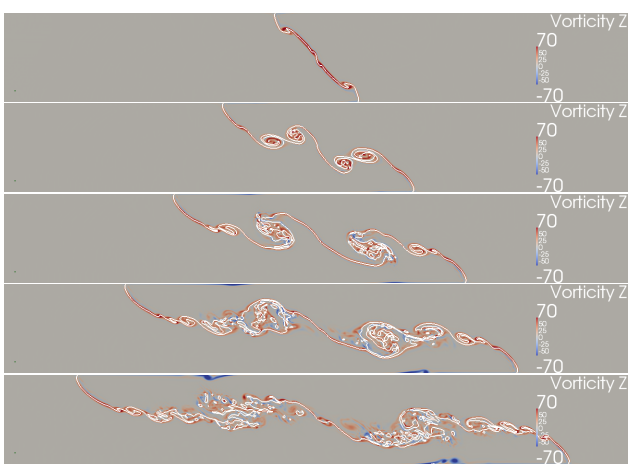

(e) $\gamma = 0.870$, $\beta = 0$

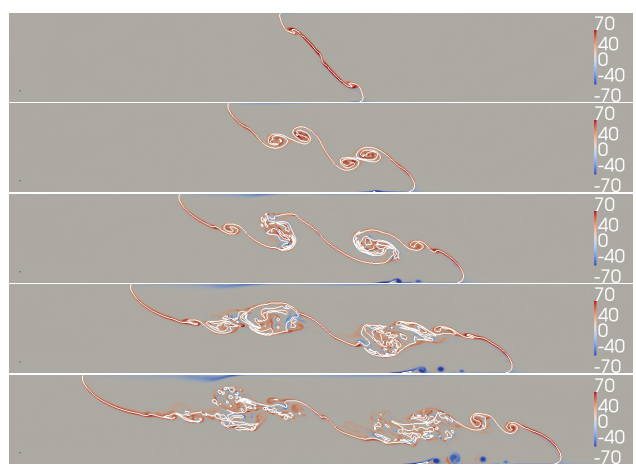

(f) $\gamma = 0.870$, $\beta = -0.57$

FIGURE 5: INTERFACE PROFILES AND VORTICITY FIELD FROM NUMERICAL SIMULATIONS OF LOCK-EXCHANGE TEST WITH DIFFERENT DENSITY RATIOS γ AND ASYMMETRY PARAMETER β. RESULTS ARE SHOWN AT NON-DIMENSIONAL TIMES $t\sqrt{g(1-\gamma)/H} = \{0.586, 1.17, 1.76, 2.34, 2.93\}$.

Copyright © 2014 by ASME

Downloaded From: http://proceedings.asmedigitalcollection.asme.org/ on 12/08/2017 Terms of Use: http://www.asme.org/about-asme/terms-of-use

the interface shear-layer into point vortices in the bulk domain of both fluids. This behaviour is the same as for the symmetric Holmboe instability mode, shown in Fig. 4b. KH-instabilities with subsequent breaking waves was not observed. This contradicts the conclusion from Benjamin's theory [27] that the presence of non-breaking regular waves at the interface of a gravity current is impossible. When the viscosity of the light fluid is increased (Fig. 5b), separation of vorticity from the interface is only observed into the heavy, less viscous fluid. The unstable wave disturbances are observed to propagate towards the front of the heavy current, i.e. in the direction of the less viscous current. This is in agreement with theory [8] and consistent with the simulation of Holmboe-waves presented in Fig. 4c. Hence, the induced disturbances travel away from the front of the lighter fluid, causing the head of the light current to be more smooth. Although the thickness of the velocity shear layer is equal to the thickness of the density transition zone initially, the former will grow with time due to viscous diffusion. Increased diffusion should be expected for turbulent shear layers.

When the density ratio is decreased to $\gamma = 0.950$, the wave disturbances in the early stage of the simulation increase in amplitude and roll up like the KH-instability (5c). At later times, the obtained light and heavy gravity currents are characterized by a front with thickness close to $H/2$, followed by a breaking interface wave due to a collapsing KH-instability. The interface between the breaking head waves of the light current and the heavy current takes the shape of an expansion wave. Small wave disturbances are seen close to the nose of the two fronts for the case with equal kinematic viscosities, but not for the case with different kinematic viscosities (cf. Fig. 5d). Entrainment from the breaking head wave is observed, both when $\delta = 1$ and when $\delta = \sqrt{10}$. A thin layer of light fluid is observed to stick to the wall below the heavy current, due to the no-slip boundary condition. This effect was also seen in direct numerical simulations of gravity currents by Härtel et al. [28].

Simulations with $\gamma = 0.870$ show more violent fluid motion (cf. Figs. 5e and 5f). Larger density difference means higher speed of the gravity current and consequently a higher Reynolds number of the flow. The initial wave disturbances here develop into double KH-billows. As for the previous case, the shape of the interface develop into the characteristic shape of such gravity currents with a thick front followed by a breaking head-wave, and an expansion-wave connecting the heavy current with the light current. Vortex shedding is observed from the lower wall-boundary at head of the heavy current. The shape of the lighter current's head is more smooth than that of the heavy current for the case of different viscosity, while the shapes are more similar for the equal viscosity case.

The Froude numbers of the lighter gravity current and the heavy currrent, Fn_L and Fn_H respectively, are defined as $Fn_L = U_L/\sqrt{(1-\gamma)gH}$ and $Fn_H = U_H/\sqrt{(1-\gamma)gH}$. According to the inviscid theory by Benjamin [27], $Fn = 0.5$ for an energy-conserving gravity current. Due to wall-friction and energy losses from wave breaking, the Froude numbers obtained from experiments are lower, and $Fn = 0.45$ is suggested by Marino et al. [29]. Froude numbers obtained with computed front speeds from the present simulations are compared with theory in Fig. 6. Deviations between numerical results and theory for the highest values of density ratio γ are believed to be an effect of Reynolds number. The computation time for a typical simulation with 590,000 grid points and 2 million time steps took about 2.5 hours on a GeForce GTX 590 graphics card.

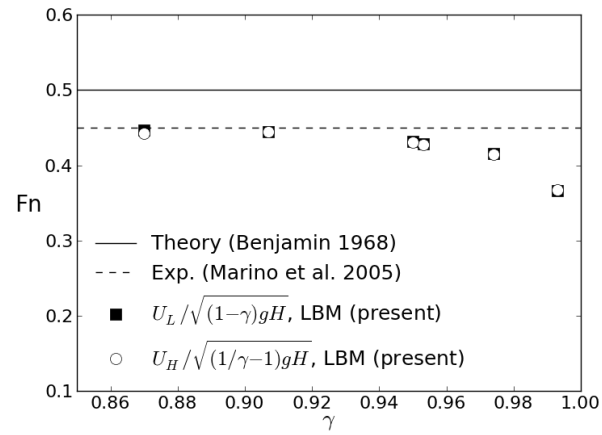

FIGURE 6: FROUDE NUMBER OF GRAVITY CURRENTS. COMPARISON BETWEEN NUMERICAL SIMULATIONS AND THEORY.

CONCLUSIONS

A numerical model based on LBM combined with a phase-field model for two-phase flow is implemented. The numerical model is verified and validated by means of several numerical tests. Obtained results show that the present numerical tool is adequate for modelling of viscous flows with immiscible fluids, where also interfacial tension is important. The model has proved to be able to capture relevant physics of stratified shear layers with fluid parameters relevant for entrainment failure of oil-booms.

ACKNOWLEDGMENT

This work is financed by the Norwegian Research Council (grant 199574/O70), Multiconsult AS and Noomas Sertifisering AS.

Copyright © 2014 by ASME

Downloaded From: http://proceedings.asmedigitalcollection.asme.org/ on 12/08/2017 Terms of Use: http://www.asme.org/about-asme/terms-of-use

REFERENCES

[1] Fingas, M., 2001. *The Basics of Oil Spill Cleanup*. Lewis Publishers.

[2] Delvigne, G. A. L., 1989. "Barrier failure by critical accumulation of viscous oil". In Proceedings of the Oil Spill Conference.

[3] Leibovich, S., 1976. "Oil slick instability and entrainment failure of oil containment booms". *Journal of Fluids Engineering - Transactions of the ASME 98,* ***1***, pp. 98–105.

[4] Thorpe, S. A., 1969. "Experiments on the instability of stratified shear flows: immiscible fluids". *Journal of Fluid Mechanics,* ***39***, pp. 25–48.

[5] Holmboe, J., 1962. "On the behavior of symmetric waves in stratified shear layers". *Geophysical Publications,* ***24***, pp. 67–113.

[6] Browand, F. K., and Winant, C. D., 1973. "Laboratory observations of shear-layer instability in a stratified fluid". *Boundary-Layer Meteorology,* ***5***, pp. 67–77.

[7] Lawrence, G. A., Browand, F. K., and Redekopp, L. G., 1991. "The stability of a sheared density interface". *Physics of Fluids,* ***A 3***, pp. 2360–2370.

[8] Pouliquen, O., Chomaz, J., and Huerre, P., 1994. "Propagating Holmboe waves at the interface between two immiscible fluids". *Journal of Fluid Mechanics,* ***266***, pp. 277–302.

[9] Smyth, W. D., and Moum, J. N., 2000. "Length scales of turbulence in stably stratified mixing layers". *Physics of Fluids,* ***12***, pp. 1327–1342.

[10] Grilli, S. T., Hu, Z., Spalding, M. L., and Liang, D., 1997. Numerical modeling of oil containment by a boom / barrier system: Phase II. Tech. rep., Department of Ocean Engingeering, University of Rhode Island, USA.

[11] He, X., and Luo, L.-S., 1997. "Lattice Boltzmann model for the incompressible Navier-Stokes equation". *Journal of Statistical Physics,* ***88***, pp. 927–944.

[12] Bhatnagar, P. L., Gross, E. P., and Krook, M., 1954. "A Model for Collision Processes in Gases. I. Small Amplitude Processes in Charged and Neutral One-Component Systems". *Phys. Rev.,* ***94***(3), May, pp. 511–525.

[13] Lallemand, P., and Luo, L.-S., 2000. Theory of the lattice Boltzmann method: Dispersion, dissipation, isotropy, Galilean invariance, and stability. Tech. Rep. 2000-17, NASA Langley Research Center, Hampton, Virginia 23681-2199, April.

[14] Brackbill, J. U., Kothe, D. B., and Zemack, C., 1992. "A continuum method for modeling surface tension". *Journal of Computational Physics,* ***100***, pp. 335–354.

[15] Jacqmin, D., 1999. "Calculation of two-phase Navier-Stokes flows using phase-field modeling". *Journal of Computational Physics,* ***155***, pp. 96–127.

[16] Cahn, J. W., and Hilliard, J. E., 1958. "Free energy of a nonuniform system. I. interfacial free energy". *Journal of Chemical Physics,* ***28***, pp. 258–267.

[17] Huang, J. J., Shu, C., and Chew, Y. T., 2009. "Mobility-dependent bifurcations in capillarity-driven two-phase fluid systems by using a lattice Boltzmann phase-field model". *International Journal for Numerical Methods in Fluids,* ***60***, pp. 203–225.

[18] Fakhari, A., and Rahimian, M. H., 2010. "Phase-field modeling by the method of lattice Boltzmann equations". *Physical Review E,* ***81***(036707).

[19] Shao, J. Y., Shu, C., and Chew, Y. T., 2012. "A hybrid phase-field based lattice-Boltzmann method for contact line dynamics". In Fourth International Symposium on Physics of Fluids (ISPF4), Vol. 19 of *International Journal of Modern Physics: Conference Series*, pp. 50–61.

[20] He, X., Shan, X., and Doolen, G., 1998. "Discrete Boltzmann equation model for nonideal gases". *Phys. Rev.,* ***57***(1), pp. 13–16.

[21] He, X., Chen, S., and Zhang, R., 1999. "A lattice Boltzmann scheme for incompressible multiphase flow and its application in simulation of Rayleigh-Taylor instability". *Journal of Computational Physics,* ***152***, pp. 642–663.

[22] He, X., and Luo, L.-S., 1997. "Theory of the lattice Boltzmann method: From the Boltzmann equation to the lattice Boltzmann equation". *Physical Review,* ***56***(6), pp. 6811–6817.

[23] Pooley, C. M., and Furtado, K., 2008. "Eliminating spurious velocities in the free-energy lattice Boltzmann method". *Physical Review E,* ***77***(046702).

[24] Schlichting, H., and Gersten, K., 2000. *Boundary Layer Theory*. Springer.

[25] Lamb, H., 1932. *Hydrodynamics*, 6th ed. Dover Publications Inc.

[26] Lowe, R. J., Rottman, J. W., and Linden, P. F., 2005. "The non-boussinesq lock-exchange problem. part 1. theory and experiments". *Journal of Fluid Mechanics,* ***537***, pp. 101–124.

[27] Benjamin, T. B., 1968. "Gravity currents and related phenomena". *Journal of Fluid Mechanics,* ***31***, pp. 209–248.

[28] Härtel, C., Eckart, M., and Necker, F., 2000. "Analysis and direct numerical simulation of the flow at a gravity-current head. part 1. flow topology and front speed for slip and no-slip boundaries". *Journal of Fluid Mechanics,* ***418***, pp. 189–212.

[29] Marino, B. M., Thomas, L. P., and Linden, P. F., 2005. "The front condition for gravity currents". *Journal of Fluid Mechanics,* ***536***, pp. 49–78.

Copyright © 2014 by ASME

Downloaded From: http://proceedings.asmedigitalcollection.asme.org/ on 12/08/2017 Terms of Use: http://www.asme.org/about-asme/terms-of-use